β-Phase poly(vinylidene fluoride) films encouraged more homogeneous cell distribution and more significant deposition of fibronectin towards the cell–material interface compared to α-phase poly(vinylidene fluoride) films

Low, Yuen Kei Adarina; Zou, Xi; Fang, Yuming; Wang, Junling; Lin, Weisi; Ng, Kee Woei; Boey, Freddy Yin Chiang

2013

Low, Y. K. A., Zou, X., Fang, Y., Wang, J., Lin, W., Boey, F., et al. (2014). β-Phase poly(vinylidene fluoride) films encouraged more homogeneous cell distribution and more significant deposition of fibronectin towards the cell–material interface compared to α-phase poly(vinylidene fluoride) films. Materials science and engineering : C, 34(1), 345-353.

https://hdl.handle.net/10356/100215

https://doi.org/10.1016/j.msec.2013.09.029

Elsevier Editorial System(tm) for Materials Science and Engineering C
Manuscript Draft

Manuscript Number: MSEC-D-13-00593R1

Title: β-Phase Poly(vinylidene Fluoride) Films Encouraged More Homogeneous Cell Distribution and More Significant Deposition of Fibronectin Towards the Cell-Material Interface Compared to α-Phase Poly(vinylidene Fluoride) Films

Article Type: Research Paper

Keywords: poly (vinylidene fluoride); polymorphism; cell-material interaction; biomaterial

Corresponding Author: Prof. Kee Woei Ng, PhD

Corresponding Author's Institution:

First Author: Yuen Kei Adarina Low

Order of Authors: Yuen Kei Adarina Low; Xi Zou; Yuming Fang; Junling Wang; Weisi Lin; Freddy Boey; Kee Woei Ng, PhD

Abstract: The piezoelectric response from β-phase poly (vinylidene fluoride) (PVDF) can potentially be exploited for biomedical application. We hypothesized that α and β-phase PVDF exert direct but different influence on cellular behavior. α- and β-phase PVDF films were synthesized through solution casting and characterized with FT-IR, XRD, AFM and PFM to ensure successful fabrication of α and β-phase PVDF films. Cellular evaluation with L929 mouse fibroblasts over one-week was conducted with AlamarBlue® metabolic assay and PicoGreen® proliferation assay. Immunostaining of fibronectin investigated the extent and distribution of extracellular matrix deposition. Image saliency analysis quantified differences in cellular distribution on the PVDF films. Our results showed that β-phase PVDF films with the largest area expressing piezoelectric effect elicited highest cell metabolic activity at day 3 of culture. Increased fibronectin adsorption towards the cell-material interface was shown on β-phase PVDF films. Image saliency analysis showed that fibroblasts on β-phase PVDF films were more homogeneously distributed than on α-phase PVDF films. Taken collectively, the different molecular packing of α and β-phase PVDF resulted in differing physical properties of films, which in turn induced differences in cellular behaviors. Further analysis of how α and β-phase PVDF may evoke specific cellular behavior to suit particular application will be intriguing.

β-Phase Poly(vinylidene Fluoride) Films Encouraged More Homogeneous Cell Distribution and More Significant Deposition of Fibronectin Towards the Cell-Material Interface Compared to α-Phase Poly(vinylidene Fluoride) Films

Y.K.A Low[a], X. Zou[a], Y.M. Fang[b], J.L. Wang[a], W.S. Lin[b], F.Y.C Boey[a] and K.W. Ng[a*]

Highlights

- PVDF films with the highest proportion of β-phase exhibited strongest piezoelectric effects and elicited highest metabolic activities in L929 fibroblasts at day 3 of culture
- β-phase PVDF induced more homogenous cell distribution compared to α-phase PVDF
- β-phase PVDF encouraged more significant fibronectin deposition towards the cell-material interface compared to α-phase PVDF
- Differences in cell physiological influences exerted by α and β-phase PVDF could be exploited for specific biomedical applications

β-Phase Poly(vinylidene Fluoride) Films Encouraged More Homogeneous Cell Distribution and More Significant Deposition of Fibronectin Towards the Cell-Material Interface Compared to α-Phase Poly(vinylidene Fluoride) Films

Y.K.A Low[a], X. Zou[a], Y.M. Fang[b], J.L. Wang[a], W.S. Lin[b], F.Y.C Boey[a] and K.W. Ng[a*]

[a] School of Materials Science and Engineering

Nanyang Technological University

N4.1 50 Nanyang Avenue

Singapore 639798

[b] School of Computer Engineering

Nanyang Technological University

N4 50 Nanyang Avenue

Singapore 639798

* Corresponding author:

Kee Woei Ng

Phone: +65 6513-8294

Fax: +65 6790-9081

Email: kwng@ntu.edu.sg

Abstract

The piezoelectric response from β-phase poly (vinylidene fluoride) (PVDF) can potentially be exploited for biomedical application. We hypothesized that α and β-phase PVDF exert direct but different influence on cellular behavior. α- and β-phase PVDF films were synthesized through solution casting and characterized with FT-IR, XRD, AFM and PFM to ensure successful fabrication of α and β-phase PVDF films. Cellular evaluation with L929 mouse fibroblasts over one-week was conducted with AlamarBlue® metabolic assay and PicoGreen® proliferation assay. Immunostaining of fibronectin investigated the extent and distribution of extracellular matrix deposition. Image saliency analysis quantified differences in cellular distribution on the PVDF films. Our results showed that β-phase PVDF films with the largest area expressing piezoelectric effect elicited highest cell metabolic activity at day 3 of culture. Increased fibronectin adsorption towards the cell-material interface was shown on β-phase PVDF films. Image saliency analysis showed that fibroblasts on β-phase PVDF films were more homogeneously distributed than on α-phase PVDF films. Taken collectively, the different molecular packing of α and β-phase PVDF resulted in differing physical properties of films, which in turn induced differences in cellular behaviors. Further analysis of how α and β-phase PVDF may evoke specific cellular behavior to suit particular application will be intriguing.

Keywords: poly (vinylidene fluoride), polymorphism, cell-material interaction, biomaterial

1. Introduction

Poly (vinylidene fluoride) (PVDF) is a semi-crystalline polymer that has found many applications due to its pyroelectric, piezoelectric and ferroelectric properties [1, 2]. Piezoelectricity refers to the interchangeable effects of mechanical and electrical stimuli on a material [3], which is known to be a property of natural composites including dentin, skin and tendon [4, 5]. The piezoelectric responses of β-phase PVDF are the highest known for any homopolymer, as a result of its high dielectric constant, crystallinity and the molecular arrangement of the fluorine atoms along the carbon backbone [6-8]. PVDF is used as a protective barrier in chemical industry applications due to its resistance to caustic chemical [9]. The technology which has allowed fabrication of PVDF with smooth surfaces made it applicable as pipe linings for handling high purity chemicals or water, since it prevents bacteria and biofilm growth [10]. Other early uses of PVDF include sensors and actuators, such as in equipment for medical ultrasonic measurements since 1979 [11]. In the biomedical context, PVDF has been used extensively as a suture material due to its high flexibility and ease of handling [10]. It is also commonly used as a membrane for immunoblotting of proteins today. Looking ahead, PVDF could find other interesting biomedical applications where its piezoelectric properties can be an advantage.

Synthetic biomaterials are often used as a supporting material or scaffold for the attachment and growth of anchorage-dependent cells. The surface properties of such templates, including topography, wettability, stiffness and chemistry not only play essential roles in cell adhesion, but also in cell differentiation. For example, fibroblasts have been shown to attach, spread and grow more rapidly on mirror-polished surfaces than micro rough titanium [12]. Using different approaches, biomaterials have been surface engineered to guide cell adhesion and modulate cell-

biomaterial interactions [13]. Moderating template stiffness and surface chemistry can also directly influence stem cell differentiation [14, 15].

The influence of a piezoelectric material or surface is intriguing and can be potentially exploited to enhance cellular interactions with a biomaterial. Research done in the 1980s showed that proteins and DNA function as piezoelectric crystal lattice structures in nature [14], which influenced transcription, translation, bone formation, adenosine triphosphate (ATP) generation, protein synthesis and membrane transport [16]. In the context of a biomaterial, Rodrigues et al. described enhanced proliferation, attachment and phosphatase alkaline activity on goat bone marrow cells seeded on β-phase PVDF membranes, especially when cultures were subjected to agitation, suggesting that this was a result of the piezoelectric property of the material [2, 17]. As a medical implant, piezoelectric materials have the potential to replace cochlear hair cells by mimicking the function of the cochlear sensory epithelium, which converts sound into electrical signals [18].

Although polarized PVDF has been reported to enhance cellular adhesion and proliferation, there are limited reports comparing the effects of PVDF polymorphism on cellular behavior, and therefore this topic remains poorly understood. In this study, we hypothesized that the intrinsic properties of α and β-phase PVDF polymorphs will elicit different cellular behaviors. Our results indicate that β-phase PVDF induced more homogeneous distribution of murine fibroblasts and encouraged more significant deposition of fibronectin towards the cell-material interface.

2. Experimental

2.1 Characterization of PVDF films

PVDF films were fabricated as described previously [19, 20]. Immersion of PVDF in 95% ethanol as anti-solvent, for 24 h, was used to remove residual solvents [1, 16, 19]. This was demonstrated to be effective using thermogravimetric analysis and preliminary cytotoxicity evaluation (data not shown). Fourier transformed Infra-red (FT-IR) measurements were done to ascertain the short range molecular arrangements at the following parameters: range 400 – 1000 cm^{-1}, resolution 1 cm^{-1}, diaphragm diameter 1 cm. The fraction of β-phase within the crystalline region was calculated using a method first described by Osaki and Ishida [19, 21]. X-ray diffraction (XRD) was recorded with a Bruker X-Ray Diffractometer (Bruker D8 Advance) using Cu K_α radiation at λ =15.54Å.

Atomic force microscopy (AFM) (DI-3100, Digital Instrument) and Piezoforce microscopy (PFM) (MFP-3D, Asylum Research) in tapping/contact mode were also used to ascertain the surface topography and piezoelectricity of the fabricated PVDF films. Piezoresponse imaging was performed over an area of 10 x 5 μm, using a conductive Pt/Ir coated Si tip with an a.c. bias of 6 V in amplitude (peak-to-peak). The out-of-plane PFM phase (OP-PFM-p) images were recorded to determine the direction of polarization. Surface morphology was assessed by scanning electron microscopy (SEM) after 80 s gold sputtering at 18 mA. SEM micrographs were taken at 3.0 kV, spot size 40 – 50.

Water contact angle measurement was performed at room temperature by sessile drop in static mode (FTA32, First Ten Ångstroms) using ultra-pure de-ionized water of volume between 1.3 to 1.9 μL, at the flow rate of 5 μL/s. Snapshots of water droplets were taken 5 s after touching

samples for equilibrium to be reached. Mean water contact angles over 5 random points on each sample were recorded, taking into account the entire drop shape.

2.2 Cell culture

Immortalized L929 murine fibroblasts between passage 5 to 20 were used to ascertain *in vitro* cell compliance, according to ASTM F813-07 standard (Standard Practice for Direct Contact Cell Culture Evaluation of Materials for Medical Devices).

PVDF films were punched into identical circular pieces (area = 2.14 cm^2), placed into a single TCPS petri dish lined with Poly dimethylsiloxane (PDMS) (Slyard® 184 Silicone Elastomer Kit, Dowing Corning) in the ratio 1:30 (curing agent/base) and dried at 37°C in vacuum over 1 week. These were sterilized by UV exposure for 20 min before cell seeding. Cells were maintained in Dulbecco's modified Eagle medium (DMEM) supplemented with 10% fetal bovine serum (FBS, Hyclone, USA), 1% penicillin-streptomycin, 1% 2 μM L-glutamine, 1% 1 mM sodium pyruvate and 1% non-essential amino acids at 37°C and 5% CO_2. Cells were allowed to proliferate in T75 flasks before harvesting at 80-90% confluence with 0.25% trypsin. Cell numbers were determined with a haemocytometer, and 1 x 10^4 cells were seeded onto each specimen in a 12-well plate, with complete DMEM. Tissue culture polystyrene (TCPS) was used as the positive control since it is widely considered the gold standard for *in vitro* cell culture experiments [22]. Phase contrast images of cells were taken at 400X magnification on an inverted light microscope (Olympus IX51), at two hour intervals post seeding, up to 12 hours, to assess cellular attachment.

2.2.1 Cell Viability and Proliferation

Cell metabolic activity and proliferation were ascertained using the AlamarBlue® (BioSource International) metabolic assay and Quant-iT™ PicoGreen® (Molecular Probes) assay respectively. All assays were performed at 1, 3, 5 and 7 days post seeding. To measure metabolic activity, fibroblasts were incubated with 0.5 mL of 10% AlamarBlue® reagent and 90% medium without FBS for 1 h at 37°C, in darkness. At the end of the incubation period, 100 μL of solution from each well was transferred (n=3) into a clean 96-well plate prior to absorbance measurement at 570 nm and 600 nm. Cell metabolic activity levels were directly correlated to percentages of reduction of AlamarBlue® reagent, which were calculated and compared against a standard calibration curve prepared in compliance with the manufacturer's recommendations.

Quant-iT™ PicoGreen® assay was used to quantify the amount of double stranded DNA (ds-DNA) present after a stipulated time of culture. Cell lysates were obtained by the addition of 1 mL 0.2% Triton X-100 at room temperature into each well, agitated on a shaker for 30 min before 50 μL of lysate (n=3) was transferred into 96-well plates. Equal amount of PicoGreen® dye, prepared in accordance to manufacturer's instruction was added into the lysate and the mixture incubated at room temperature for 5 min in darkness. Fluorescence was measured at an excitation wavelength of 485 nm and emission wavelength of 535 nm, on a microplate reader (Tecan). Cultures of L929 fibroblasts with known cell numbers were used to obtain a straight line calibration curve in order to correlate the corresponding cell number on each sample.

2.2.2 Immunocytochemistry

At stipulated timepoints, samples were washed with phosphate buffer saline (PBS) before cell fixation with 4% paraformaldehyde (PFA) in PBS at 4°C overnight. Cells were rinsed thrice with PBS for 10 min each on a shaker to remove residual PFA. Fixed cells were permeabilized with 0.1% Triton X-100 in PBS at room temperature for 15 min. In order to reduce non-specific background, samples were treated with a blocking solution (1% BSA and 10% goat serum) for 30 min at 37°C. Identification of fibronectin (FN) deposition was performed by immunocytochemical labeling using rabbit anti-mouse FN IgG (1:100; AB2413, Abcam) followed by probing with Alexa Fluor 488 conjugated goat anti-rabbit IgG (1:500; A11034, Invitrogen) for 1 h each at room temperature. F-actin was stained for 20 min with Alexa Fluor 568 conjugated phalloidin (Invitrogen) at a dilution of 1:40 in PBS/BSA at 37°C, in the dark. Nuclei were counterstained with DAPI (Invitrogen) for 5 min at room temperature, in the dark. Samples were mounted onto glass slides and cover-slipped with DAKO fluorescent mounting medium before viewing under a fluorescence microscope (Nikon) or confocal microscope (Leica TCS SP5).

2.2.3 Scanning Electron Microscopy and Saliency Test

The morphology and distribution of cells cultured over various timepoints on the PVDF films were evaluated by SEM after fixation with 2.5% glutaraldehyde (Sigma Aldrich). Dehydration was carried out step-wise in increasing ethanol concentrations from 50% to 100%, for 10 min each step at room temperature. The affinity of cells towards each of these films was determined by taking multiple SEM micrographs for cell morphology evaluation.

Saliency test was conducted on SEM images to make comparisons of fibroblasts distribution on the two PVDF polymorphs studied (n=20). Protocol of the computer-assisted mapping approach consisted of 2 stages: thresholding and cell identification. Surface morphological background of PVDF films sharing similar morphology features with fibroblasts was suppressed by thresholding. The saliency of grey-scaled images was sectioned into 0.05 degree for computation of intensity results, and thus the level of significance from each point is 0.05. Clusters of cells were viewed as more pronounced points with higher saliency when compared to surrounding regions where cells were flat and spread. Statistical results of the intensity values in saliency maps were obtained from the MATLAB computing algorithm and plotted as frequency versus intensity.

2.2.4 Statistical Analysis

Statistical analyses were performed using Statistical Package for the Social Sciences (SPSS) version 20.0. Results were analyzed for statistical significance using one way analysis of variance (ANOVA) with 95% confidence interval, followed by post hoc procedure (Tukey's test). A p-value of less than 0.05 was considered to be significant. Analyses of fluorescence images were done using Image J software.

3. Results

3.1 Characterization by FT-IR and XRD

The FT-IR spectra of fabricated PVDF films were recorded and presented in *Figure 1A*. DMF-PVDF and DMAc-PVDF dried at 140°C showed prominent α-phase peaks at 615 cm^{-1}, 764 cm^{-1}

and 976 cm^{-1}, while β-phase peak at 840 cm^{-1} were most evident in HMPA-PVDF films dried at 140°C. By using the method discussed previously [19], the relative fraction of β-phase [F(β)] PVDF in the films were calculated. Congruent to our previous study, the F(β) of DMF-PVDF and DMAc-PVDF films dried at 60°C were between 73.93% and 85.95% within the crystalline regions. When drying temperature was increased to 140°C, F(β) of these two groups dropped to between 18.04% and 35.84%. However, the F(β) of HMPA-PVDF dried at 140°C remained above 90%, in agreement with our previous data [19].

Results from XRD analysis of DMF-PVDF and DMAc-PVDF dried at 140°C showed distinct peaks at 18.4° and 19.9°, corresponding to crystal planes at (020) and (110) of α-phase PVDF (*Figure 1B*) [23]. These peaks were negligible in other spectra where the F(β) was significantly higher. HMPA-140 films most strongly expressed the characteristic β-phase peaks at 20.3°.

3.2 Characterization of PFM results

To quantify the piezoelectric response of our PVDF films, a consistent a.c. bias of 6 V was applied to the tip during the sample scanning. Commercially available PVDF-TrFE (poled) was used as the positive control while PET acted as the negative control. The OP-PFM-p images (*Figure 2A*) confirmed that regions of β-phase exhibited piezoelectric properties. Compared with the positive control, the largest piezoelectric area came from HMPA-140 films, which had more than 90.0% β-phase within the crystalline region. DMF-140 and DMAc-140, which were previously calculated to have the least amount of β-phase PVDF, showed uniform phase distribution throughout the scanned area that was similar to non-piezoelectric PET, indicating the absence of β-phase PVDF.

The plots of distribution of polarization direction (*Figure2B*) showed sharp peaks for all PVDF films, but peak broadening towards negative voltage region was only observed for β-phase PVDF films, indicating upwards polarization. Congruent to our results from the FT-IR calculations, HMPA-140 had the highest proportion of polarized β-phase.

3.3 Surface topography, roughness and water contact angle

Surface topographies were observed under the SEM while AFM recorded the average surface roughness (*Figure 3A-B*). For DMF-60 and DMAc-60 PVDF films, the mean roughness recorded was between 55.7 ± 4.6 nm to 60.8 ± 5.9 nm, compared to 291.0 ± 4.7 nm for HMPA-140 film. Polarized microscopy images confirmed the formation of spherulites in PVDF films (*Figure 3C*). The spherulites grew in size when drying temperature increased from 60°C to 140°C, with the most apparent increase observed for DMAc-140. The mean roughness of DMAc-140 was 860.0 ± 7.1 nm, higher than that of DMF-140, at 222.0 ± 6.3 nm.

Contact angle measurements were performed to compare the hydrophilicity of fabricated PVDF films before cell culture studies. Our results showed that contact angles were statistically higher for DMF-60 and DMAc-60 films (*Figure 3D*; $p<0.05$). The rest hovered between the ranges 73.16 ± 3.1° to 78.74 ± 2.9° and were statistically indifferent. All PVDF films prepared were statistically more hydrophobic than TCPS which recorded a contact angle of 66.06 ± 1.0°.

From our characterization results, the PVDF films were classified as having majority α or β-phase PVDF, denoted in parentheses as follows: DMF-140(α), DMAc-140(α), DMF-60(β),

DMAc-60(β) and HMPA-140(β). This classification allows us to investigate the influence of the two polymorphs on cellular behavior.

3.4 Cell Proliferation and Metabolic Activity per Cell

Fibroblasts seeded were monitored with phase contrast light microscopy for the formation of filopodia and lamellipodia, as indications of adhesion, from the point of seeding up to 12 h (*results not shown*). Cells typically took between 2 to 4 h to adhere onto TCPS surface, but up to 12 h before attachment on PVDF films. The proliferation profiles and metabolic activity per cell of L929 fibroblasts cultured on PVDF films and TCPS over one-week were presented in *Figure 4*. As adhesions were weak and incomplete at day 1, biological assay may not portray accurate metabolic activity and proliferation of fibroblast. Therefore, the assays were not carried out on day 1.

Proliferation of L929 fibroblasts from days 3 to 7 was measured by quantifying DNA using the PicoGreen™ assay and normalizing to TCPS (*Figure 4A*). No significant differences were observed between the numbers of fibroblast on all PVDF films at each timepoint, except for DMAc-140(α) which registered lower cell numbers across all timepoints. Metabolic activity per cell was calculated with the AlamarBlue® assay and normalized to DNA quantity from the proliferation data (*Figure 4B*). With increasing number of fibroblasts, metabolic activity per cell dropped, possibly due to contact inhibition. Cell metabolic activity on HMPA-140(β), the group with the highest proportion of β-phase PVDF, was significantly higher than all other PVDF films at day 3 of culture, although this difference was lost after day 3. Conversely, cell metabolic

activity on DMAc-140(α), the group with the lowest proportion of β-phase PVDF, was lower than the other PVDF groups at day 5 of culture.

3.5 Scanning Electron Microscopy, Saliency Mapping and Fibronectin Expression

Representative SEM images of fibroblasts fixed at stipulated timepoints were taken to evaluate differences in cell morphology on the different PVDF films. At day 1, cells were few and far between, an indication that fibroblast were weakly attached and may have been washed off due to the rinsing and dehydration procedures undertaken. On day 3 when cell densities were low, the morphology of fibroblasts on all PVDF films were indifferent. Spindle, triangular and polygonal cells were observed, typical of fibroblasts cultured on TCPS. In addition, fibroblasts also appeared as clusters of round cells on α-phase (DMF-140 and DMAc-140) PVDF. By day 5, cell densities had increased by at least 5 folds from day 3, as shown in *Figure 4A*. As cell densities increased, cell morphology on the α-phase PVDF films became distinct from those on the β-phase PVDF films. By day 7, random clustering of fibroblasts was prominent on α-phase PVDF films, with single cells appearing to migrate out of these clusters. On the contrary, fibroblasts on DMF60(β), DMAc-60(β) and HMPA-140(β) were considerably more spread out (*Figure 5A*). From the SEM images, spreading of fibroblasts was indifferent on DMF60(β) compared to DMAc60(β) while cells were harder to distinguish on HMPA140(β) due to higher surface roughness. Fibroblasts on TCPS were confluent at day 7 of culture but did not cluster in the manner observed on the PVDF films.

Saliency test was conducted, with statistical accuracy up to 0.05 intensity in grey-scaled images, to quantify the extent of differences in cellular distributions between α and β-phase PVDF films

at day 7 (n = 20). Results revealed that the distribution and morphology of fibroblasts on β-phase PVDF resembled that on TCPS control group, in contrast to α-phase PVDF. Cell morphology and spreading were similar on both the α-phase PVDF films *(Figure 5B)*.

Immunocytochemical staining of fibronectin (FN) was carried out to evaluate the distribution of cell secreted extracellular matrix proteins. The cross sectional views of the samples assembled from z-stacked confocal images showed that on α-phase dominant PVDF films, FN was distributed relatively homogeneously throughout the depth of the samples (*Figure 6*). However, FN distribution on all β-phase dominant PVDF films showed higher concentration towards the cell-material interface.

4. Discussion

Many biological applications of materials require improving or preventing cell adhesion for different purposes. In PVDF, we hypothesized that due to the intrinsic properties of the α and β-phase polymorphs, cellular behavior on these two surfaces would be different. In this study, we followed up on our earlier report [19] to evaluate more specifically the differences in cellular behavior that α and β-phase PVDF may evoke.

From our FT-IR and XRD characterization results, DMF-140 and DMAc-140 films had majority α-phase PVDF while DMF-60, DMAc-60 and HMPA-140 films had majority β-phase PVDF. Although α and β-phase PVDF are similar to each other in the 2θ values of X-ray diffractions [24], our results confirmed the differences in polymorphic phases based on existing literature [25-31].

Theoretically, PVDF polymer is an insulator of electricity, especially at the amorphous regions. When an insulator is subjected to a.c. bias during PFM scanning, charge accumulation occurs at the surface. Charge accumulation creates electrostatic force between the tip and sample to result in an artificial phase shift towards the positive voltage direction, as seen in the graphs of all PVDF films tested (*Figure 2B*). Polarization in the upwards direction were recorded but polarization in the downwards direction were masked by the charge accumulation effect, and therefore cannot be distinguished for all PVDF films tested. Our PFM results showed that HMPA-140(β) films exhibited the largest piezoelectric area among the films tested, while α-phase PVDF polymorph films did not exhibit piezoelectric property.

PVDF polymorphism was shown to play a more significant role in determining the water contact angle than surface roughness in *Figure 3*. The significantly lower surface roughness of DMF60 and DMAc60 β-phase PVDF films were more hydrophobic compared to all the other PVDF films. However, when comparison was done between DMF-140(α) and HMPA-140(β), lower surface roughness of DMF-140(α) did not translate into higher hydrophobicity. Instead, the water contact angle of DMF-140(α) and DMAc-140(α) were not significantly different even though DMAc-140(α) recorded the highest surface roughness (860 ± 7.1 nm). Therefore, wettability of PVDF is more closely related to polymorphism than surface roughness. Wettability of a substrate is also associated to the surface energy. It was reported that crystalline polymers, being more hydrophobic, has higher surface energy than amorphous polymer. It was also reported that increasing protein adsorption on surfaces with higher energy allows cell spreading [32].

Fibroblasts are common in connective tissues that adhere to the extracellular matrix (ECM) through bio-specific interactions. In a study conducted by Wei et al., L929 mouse fibroblasts were seeded on hexamethyldisiloxane (HMDSO) surfaces modified by oxygen plasma treatment

to attain wettability between 0° to 106° [33]. Their results revealed that initial fibroblasts attachment were higher on hydrophilic surfaces but proliferation rate was not affected for wettability between 0° to 80°. On the contrary, our results also showed no difference in initial attachment of fibroblasts on all PVDF films between the points of seeding up to 12 hours. However, proliferation of L929 was in agreement to the results presented by Wei et al. Since the measured water contact angle of our fabricated α and β-phase PVDF films were close to the range studied, we concluded that surface wettability did not result in the differences in proliferation rate observed on α and β-phase PVDF films. On the contrary, Chen et al. reported that the wettability of a surface affects the initial attachment of cells and protein adsorption onto the substrate surface, while hydrophobicity inhibited cellular proliferation but not adhesion [34]. Likewise, Park and Cima also reported lower growth rate of 3T3 fibroblasts on crystalline substrate, that was hydrophobic [32]. However, the slight difference in contact angle between each fabricated PVDF films in our experiment was insufficient to cause prolonged initial cellular attachment, since our results showed that fibroblasts seeded on both α and β-phase PVDF films took more than 12 h before attachment. Even though the proliferation rates were similar on the PVDF films tested, cell morphology was different on α and β-phase polymorphs.

It is known that surface roughness plays a role in influencing cellular distribution, and fibroblasts are known to spread less on rough and more on smooth surface, due to mechanical stabilization [12]. Fibroblasts seeded on rough surfaces are supported by ridges and pitches and thus do not have to express distinctive F-actin network. On the other hand, fibroblasts on smooth surface need to develop a strong network to stabilize on the surface. When comparison was done between DMAc-60(β) and HMPA-140(β) of surface roughness 60.8 ± 5.9 nm and 291.0 ± 4.7 nm respectively, the significantly different roughness values did not cause any significant effects

on cellular distribution as observed from saliency mapping results (*Figure 5*). Instead, our saliency mapping and SEM images suggested that fibroblasts seeded on α-phase PVDF films were clustered while fibroblasts on β-phase films were spread. This implied that surface roughness within this range studied did not result in differential cell behavior on films with similarly high proportion of β-phase PVDF, based on the assays used.

Likewise, on PVDF films of predominant α-phase, DMF-140(α) and DMAc-140(α) where surface roughness were 222.0 ± 6.3 nm and 860.0 ± 7.1 nm respectively, saliency mapping results and cross-sectional fibronectin distributions did not reveal significant differences in cell spreading patterns and fibronectin (FN) deposition. It suggests that surface topography differences between these films did not affect these two aspects of cell behavior.

Meanwhile, DMF-140(α) and HMPA-140(β) films with significantly different PVDF polymorph proportions but relatively similar surface roughness (222.0 ± 6.3 nm vs 291.0 ± 4.7 nm) resulted in clear differences in cellular behavior. Saliency mapping and cross sectional FN distribution showed that HMPA-140(β) induced higher degree of fibroblast spreading and more FN deposition towards the cell-material interface than DMF-140(α). This suggests that protein adsorption on β-phase PVDF was likely more significant than on α-phase films. Consequently, cells proliferated in clusters on α-phase dominant films. PVDF polymorphism therefore appeared to play a more significant role than surface roughness in determining cellular distribution and FN deposition pattern by fibroblasts.

In summary, our results indicated that β-phase PVDF induced more homogeneous distribution of L929 murine fibroblasts and encouraged more significant deposition of FN towards the cell-material interface.

5. Conclusion

In this study, we investigated the differential effects that α and β-phase PVDF may exert on L929 murine fibroblasts. In agreement with the literature, films with majority β-phase PVDF exhibited greater piezoelectric characteristics compared with films with majority α-phase PVDF. Comparative assays for proliferation rate and metabolic activity of L929 fibroblasts on the films samples showed no significant influence of surface roughness within the range studied. Consequently, our results suggest that PVDF films of predominant β-phase induced more homogeneous cell distribution and increased fibronectin deposition towards the cell-material interface. In essence, the difference in molecular packing of α and β-phase had resulted in different piezoelectric properties in the films, which in turn induced different cellular behaviors. These findings could be significant in exploiting novel biomedical applications of PVDF where the ability to modulate piezoelectric properties in a single material could be advantageous.

Acknowledgement

The authors would like to thank Miss Gou Rui for the helpful discussions on PFM image analysis.

Vitae

Yuen Kei Adarina Low received her PhD from the School of Materials Science and Engineering, Nanyang Technological University, Singapore in 2013. Her thesis – "Material characterization and cellular behavior on different poly (vinylidene fluoride) polymorphs" explored the effects of PVDF polymorphism on metabolic and proliferation behavior on murine fibroblast. Her current research is on blood pathogen detection for water remediation.

Zou Xi received his PhD from Nanyang Technological University in 2013. He is currently a application scientist in Nanometrics. During PhD study, he worked on the switching mechanism and fatigue mechanism for the next generation non-volatile memories based on perovskite oxides. His expertise is on the SPM techniques (EFM, SKPM and PFM) for local electrical properties of oxide thin films and planar device fabrication.

Yuming Fang is a Ph.D. student in the School of Computer Engineering, Nanyang Technological University in Singapore. Previously, he obtained B.E. and M.S. from Sichuan University and Beijing University of Technology, China, respectively. From October 2011 to January 2012, he was a visiting Ph.D. student in National Tsinghua University, Taiwan. From September 2012 to December 2012, he was a visiting scholar in University of Waterloo, Canada. His research interests include visual attention modeling, visual quality assessment, image retargeting, computer vision, 3D image/video processing, etc. He was a special session organizer in VCIP 2013.

Junling Wang received his PhD from University of Maryland, College Park in 2005. He joined the School of Materials Science and Engineering, NTU in March 2006. He is currently an Associate Professor in the Materials Science division. His research focuses on multifunctional oxide thin films and their applications in nanoelectronic and spintronic devices. Through materials processing, structural analysis and property characterizations, he tries to understand the fundamental physics of functional oxides and develop new materials/devices for the next generation nanotechnology. He has published 75 papers in high impact journals, including Science, Nature Communications, and Advanced Materials. His work has been cited for >4200 times.

Weisi Lin received his Ph.D. from King's College London. His research interests include image processing, perception-inspired signal modeling and multimedia communication. He has published 240+ refereed papers in international journals and conferences. He is Associate-Editors of IEEE Trans. on Multimedia, IEEE SIGNAL PROCESSING LETTERS and *Journal of Visual Communication and Image Representation*. He is a Technical Program Chair for *IEEE ICME* 2013, and the Lead Technical Program Chair for PCM 2012. He has been elected as a Distinguished Lecturer of APSIPA (2012-2013). He is a Fellow of Institution of Engineering Technology, and an Honorary Fellow, Singapore Institute of Engineering Technologists.

Professor Freddy Boey is the Provost, NTU. Scientist, researcher, inventor and educator, Professor Boey is a serial inventor and founded several companies through some of his

inventions like the fully biodegradable and dual drug eluting heart stents, biodegradable PDA/PFO/ASD occluders, FDA approved PVDF Hernia mesh and disposable tissue retractors, a miniature piezoelectric heart pump, sustain drug release for Glaucoma using liposome etc. His fully biodegradable stent, PDA/PFO/ASD occluders and glaucoma drug delivery device are currently undergoing human trials in Columbia, India and Singapore, respectively. He has won more than $36m in research grants in the last three years and received many prestigious awards, including Singapore's Public Administration Medal (Silver) in 2010, honorary doctorate from Loughborough University and Faculty of Medicine Fellowship at Imperial College.

Kee Woei Ng received his PhD from the Yong Loo Lin School of Medicine, National University of Singapore, in 2006 and is currently an Assistant Professor at the School of Materials Science and Engineering at Nanyang Technological University. His research focusses on cell-material interactions within the scopes of tissue engineering, regenerative medicine and nanotoxicology. He is specifically interested in developing biomaterials and establishing fundamental understanding of how materials influence cell physiology in ways that can be exploited for relevant applications. His work has been published in top biomaterials journals and has been cited more than 1000 times.

References

[1] Gaurav Mago, Dilhan M. Kalyon, F.T. Fisher, Journal of Nanomaterials, 2008 (2008) 8 pages.

[2] Ribeiro C., Panadero J.A., Sencadas V., S. Lanceros-Mendez, Tamano M.N., Moratal D., Salmeron-Sanchez M., G.R. J.L, Biomedical Materials, 7 (2012).

[3] Z.-Y. Wang, K.-H. Su, H.-Q. Fan, Z.-Y. Wen, Polymer, 49 (2008) 2542-2547.

[4] E. Fukada, Ieee Transactions on Ultrasonics Ferroelectrics and Frequency Control, 47 (2000) 1277-1290.

[5] T. Wang, Z. Feng, Y. Song, X. Chen, Dental Materials, 23 (2007) 450-453.

[6] C.S. Lovell, J.M. Fitz-Gerald, C. Park, Journal of Polymer Science Part B-Polymer Physics, 49 (2011) 1555-1562.

[7] P. Guthner, D. K., Applied Physics Letters, 61 (1992) 1137-1139.

[8] V. Piefort, in: Department of Mechanical Engineering and Robotics, Universite Libre de Bruxelles, Brussels, 2001, pp. 126.

[9] H. Teng, Applied Sciences, 2 (2012) 496-512.

[10] S. Kakoei, F. Baghaei, S. Dabiri, M. Parirokh, S. Kakooei, Iranian Endodontic Journal, 5 (2010) 69-73.

[11] R.C. Eggleton, T. McGlinn, in: Proceeding of the 24th Annual Convention on American Institute of Ultrasound in Medicine AIUM, 123, Laurel, MD, 1979.

[12] T.P. Kunzler, T. Drobek, M. Schuler, N.D. Spencer, Biomaterials, 28 (2007) 2175-2182.

[13] Z.W. Ma, Z.W. Mao, C.Y. Gao, Colloids and Surfaces B-Biointerfaces, 60 (2007) 137-157.

[14] A.J. Engler, S. Sen, H.L. Sweeney, D.E. Discher, Cell, 126 (2006) 677-689.

[15] C.Y. Tay, H.Y. Yu, M. Pal, W.S. Leong, N.S. Tan, K.W. Ng, D.T. Leong, L.P. Tan, Experimental Cell Research, 316 (2010) 1159-1168.

[16] Y.K.A. Low, L.Y. Tan, L.P. Tan, F.Y.C. Boey, K.W. Ng, Journal of Applied Polymer Science, 128 (2012) 2902-2910.

[17] M.T. Rodrigues, M.E. Gomes, J.F. Mano, R.L. Reis, beta-PVDF Membranes Induce Cellular Proliferation and Differentiation in Static and Dynamic Conditions, in: Advanced Materials Forum Iv, 2008, pp. 72-76.

[18] J. Ashmore, Physiological Reviews, 88 (2008) 173-210.

[19] Y.K.A. Low, M. N, N.D. Niphadkar, F.Y.C. Boey, K.W. Ng, Journal of Biomaterials Science, Polymer Edition, 22 (2011) 1651-1667.

[20] M. Benz, W.B. Euler, Journal of Applied Polymer Science, 89 (2003) 1093-1100.

[21] S. Osaki, Y. Ishida, Journal of Polymer Science Part B-Polymer Physics, 13 (1975) 1071-1083.

[22] N. Weber, Y.S. Lee, S. Shanmugasundaram, M. Jaffe, T.L. Arinzeh, Acta Biomaterialia, 6 3550-3556.

[23] B.A. Newman, C.H. Yoon, K.D. Pae, J.I. Scheinbeim, Journal of Applied Physics, 50 (1979) 6095-6100.

[24] Park YJ, Kang YS, P. C, European Polymer Journal, 41 (2005) 1002-1012.

[25] R. Gregorio, E.M. Ueno, Journal of Materials Science, 34 (1999) 4489-4500.

[26] D.J. Lin, H.H. Chang, T.C. Chen, Y.C. Lee, L.P. Cheng, European Polymer Journal, 42 (2006) 1581-1594.

[27] V. Sencadas, S. Lanceros-Mendez, J.F. Mano, Thermochimica Acta, 424 (2004) 201-207.

[28] R. Gregorio, Journal of Applied Polymer Science, 100 (2006) 3272-3279.

[29] A. Park, L.G. Cima, Journal of Biomedical Materials Research, 31 (1996) 117-130.

[30] A. Salimi, A.A. Yousefi, Polymer Testing, 22 (2003) 699-704.

[31] R. Hasegawa, Takahash.Y, H. Tadokoro, Y. Chatani, Polymer Journal, 3 (1972) 600-610.

[32] A.J. Salgado, Y. Wang, J.F. Mano, R.L. Reis, Influence of molecular weight and cristallinity of poly(L-lactic acid) on the adhesion and proliferation of human osteoblast like cells, in: Advanced Materials Forum Iii, Pts 1 and 2, 2006, pp. 1020-1024.

[33] J. Wei, M. Yoshinari, S. Takemoto, M. Hattori, E. Kawada, B. Liu, Y. Oda, Journal of Biomedical Materials Research Part B: Applied Biomaterials, 81B (2007) 66-75.

[34] Chen RS, Chen YJ, Chen MH, Y. TH, Journal of Biomedical Materials Research Part A., 83A (2007) 241-248.

Figure 1 Characterization of PVDF polymorphs. (A) FT-IR spectral showed prominent α-PVDF peaks for DMF-140 and DMAc-140 films. β-PVDF peaks were most evident in HMPA-140 films. In agreement with FT-IR results, (B) XRD diffractograms of PVDF films showed that DMF-140 and DMAc-140 films expressed the characteristic α-PVDF peaks (18.4° and 19.9°) most prominently while HMPA-140 films most strongly expressed the characteristic β-PVDF peaks (20.3°).

Figure 2 PFM analysis of piezoelectric properties on PVDF films. (A) The OP-PFM-p signal of PVDF films showed distinct positions exhibiting piezoelectric responses on films dominated by β-phase PVDF. Commerically available PVDF-TrFE and PET films were used as positive and negative controls, respectively. (B) Plots of direction of polarization showed a single sharp peak for all PVDF films. Broadening of this peak towards the negative voltage was observed only for β-phase PVDF films.

Figure 3 Surface properties characterization of PVDF films. (A) SEM and corresponding (B) AFM images of the 5 PVDF films showed distinct variations in their surface topographies. (C) Polarizing light microscopy confirmed the formation of spherulites on the PVDF films. (D) The average contact angle and surface roughness of the PVDF films are tabulated (n=3). Mean roughness values were independent on PVDF polymorphism, but contact angle measurements showed that films of majority β-phase PVDF were generally more hydrophobic than those made of majority α-phase PVDF.

Figure 4 Cell proliferation and metabolic activity on PVDF films over 7 days. (A) No significant differences in cell number were recorded on the different films except on DMAc140-α which registered significantly lower cell number than other samples at every time point. (B). Metabolic activity per cell decreased as cell number increased. However at day 3, metabolic activity per cell was significantly higher on HMPA140-β compared to the other PVDF films, although this was lower than on TCPS. (*$p<0.05$; ANOVA and Tukey's test)

Figure 5 (A) SEM analysis was carried out to evaluate L929 fibroblast morphology on PVDF films over 7 days. As cell densities increased due to proliferation, aggregated cell clusters began to appear on PVDF films. This was most pronounced on DMF140 and DMAc140 samples at day 7. (B) Saliency analysis of SEM images (n=20) of PVDF samples cultured with L929 fibroblasts for 7 days. Fibroblasts seeded on α-phase displayed stronger cell-cell interaction, while morphology of fibroblasts resembled that of TCPS control.

Figure 6 Fibronectin expression on PVDF films. Confocal laser microscopy images of sample cross sections showed fibronectin expression (green) across the cell layers. The corresponding plots of the relative expression levels of fibronectin across the vertical depths of cell layers are shown. Fibronectin expression on films of predominately β-phase PVDF was more pronounced towards cell-material interface.

Figure(s)

Figure 1

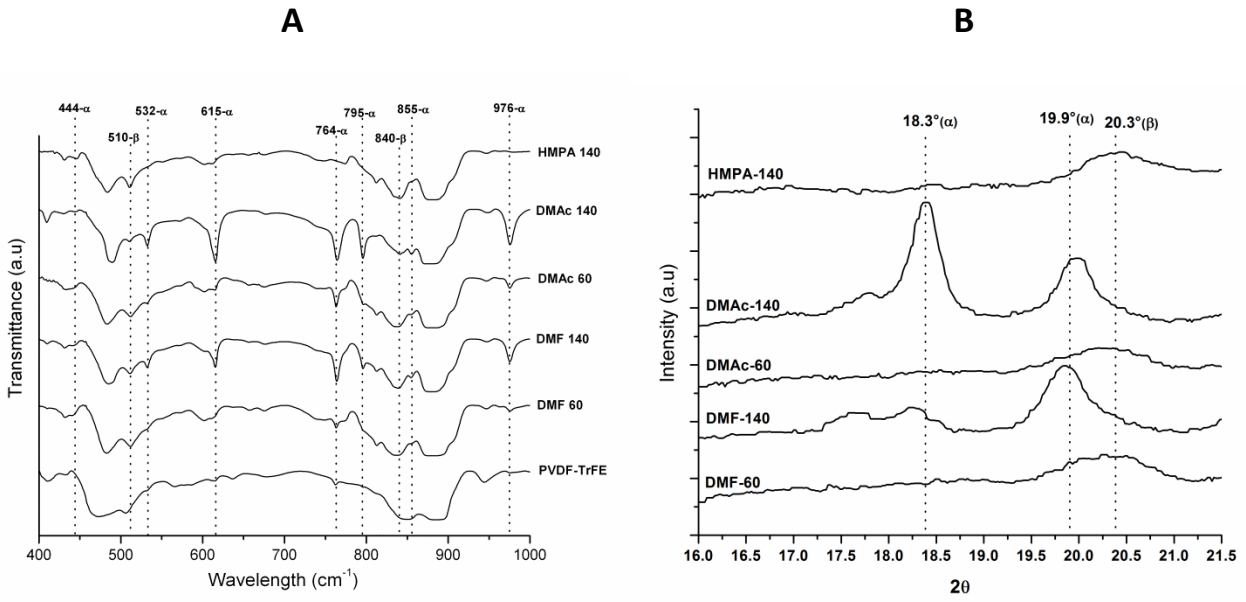

Figure 2

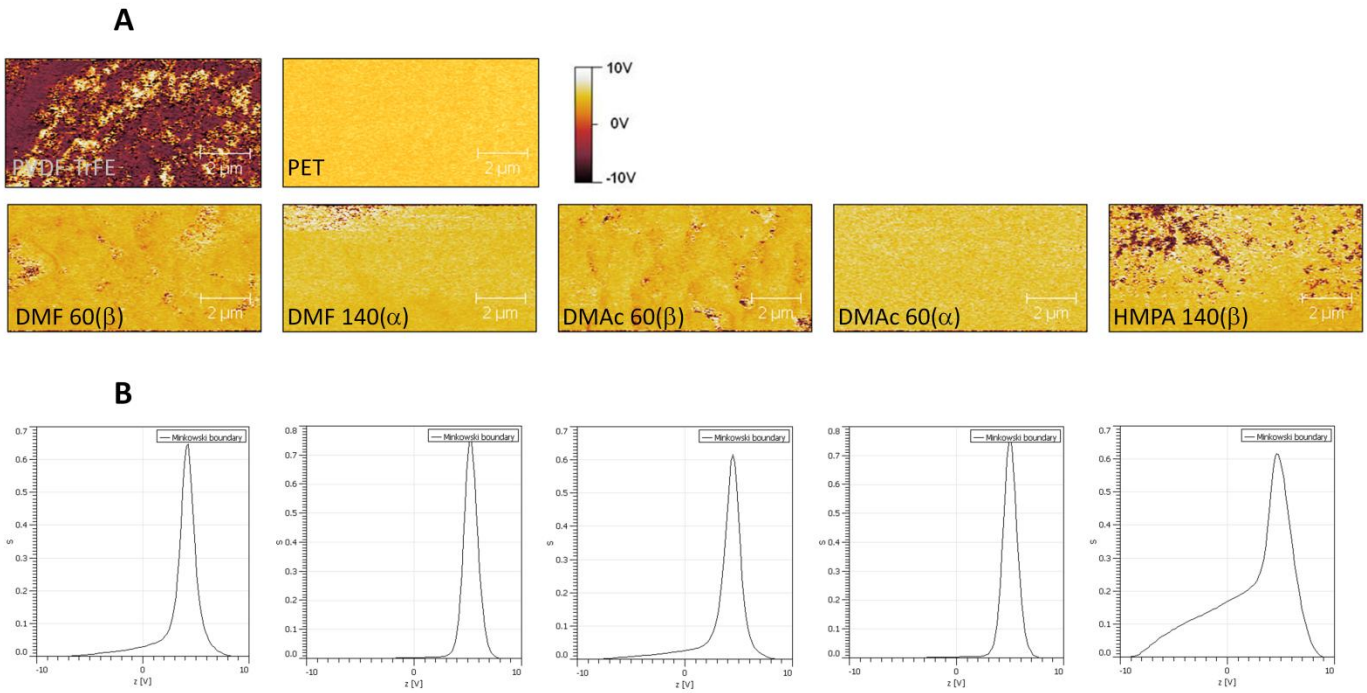
A
PVDF-HFE
2 µm
PET
2 µm
10V
0V
-10V
DMF 60(β)
2 µm
DMF 140(α)
2 µm
DMAc 60(β)
2 µm
DMAc 60(α)
2 µm
HMPA 140(β)
2 µm
B
Minkowski boundary
s
z [V]

Figure 3

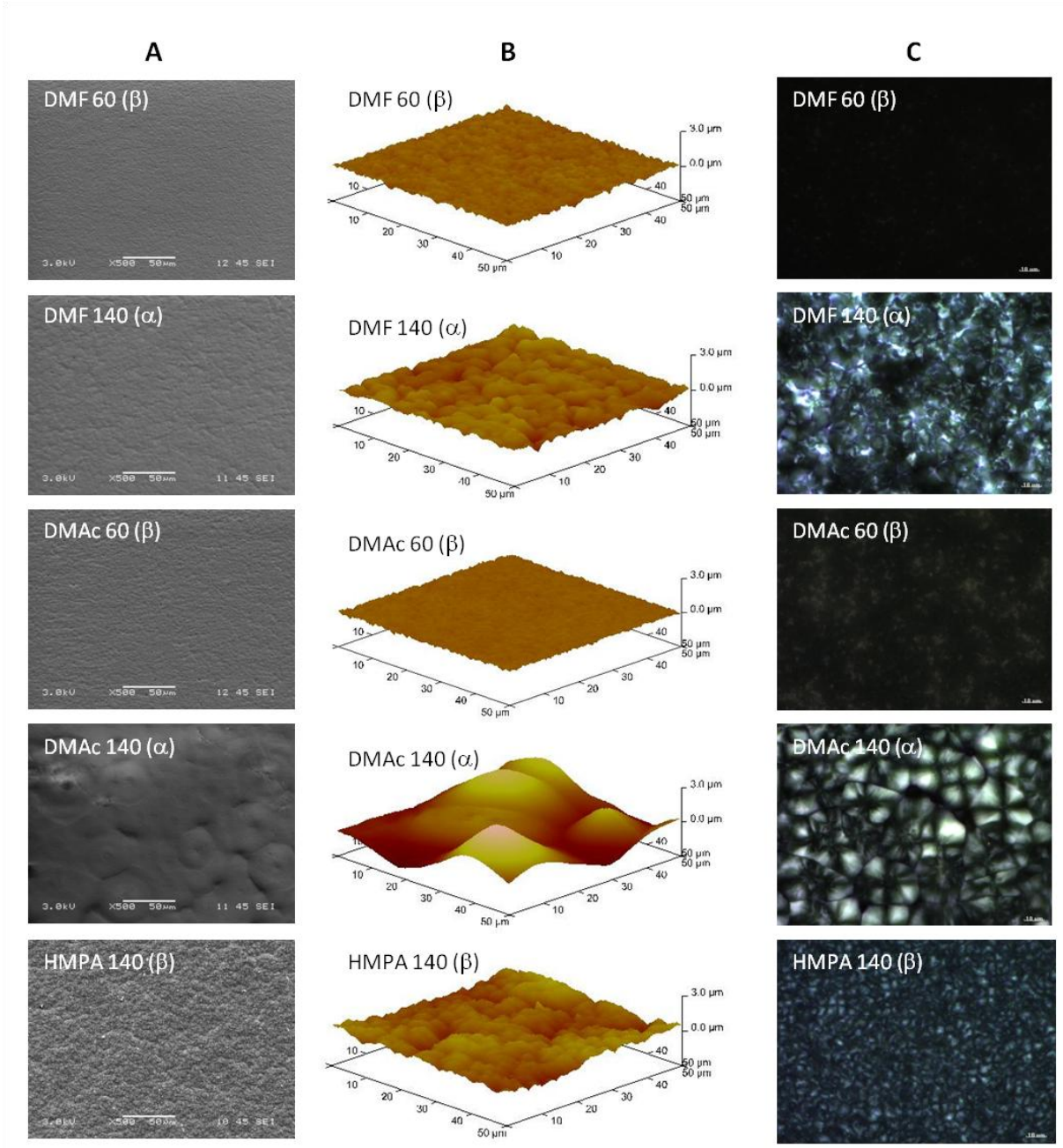

D

Sample	Average Contact Angle ( )	Surface Roughness (nm)
DMF-60	84.79 3.5	55.7 4.6
DMF-140	73.16 3.1	222.0 6.3
DMAc-60	85.48 3.4	60.8 5.9
DMAc-140	74.48 1.4	860.0 7.1
HMPA-140	78.74 2.9	291.0 4.7
TCPS	66.06 1.0	18.4 0.41

Figure 4

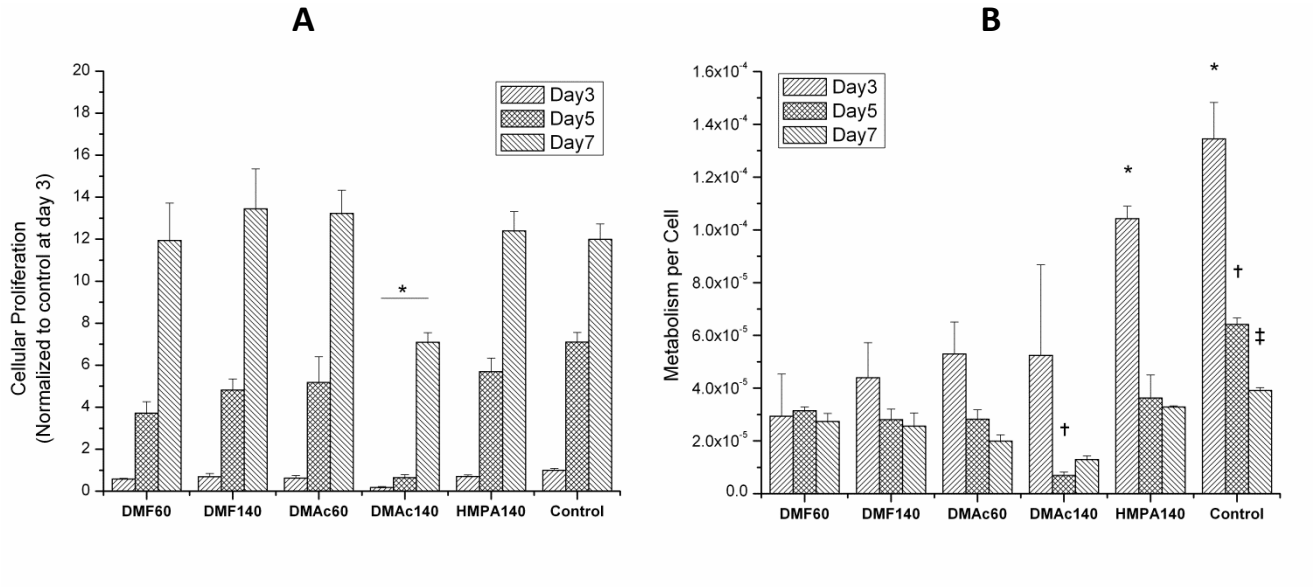
A
Cellular Proliferation
(Normalized to control at day 3)
Day3
Day5
Day7
*
DMF60
DMF140
DMAc60
DMAc140
HMPA140
Control
B
Metabolism per Cell
Day3
Day5
Day7
*
†
‡
DMF60
DMF140
DMAc60
DMAc140
HMPA140
Control

Figure 5

A

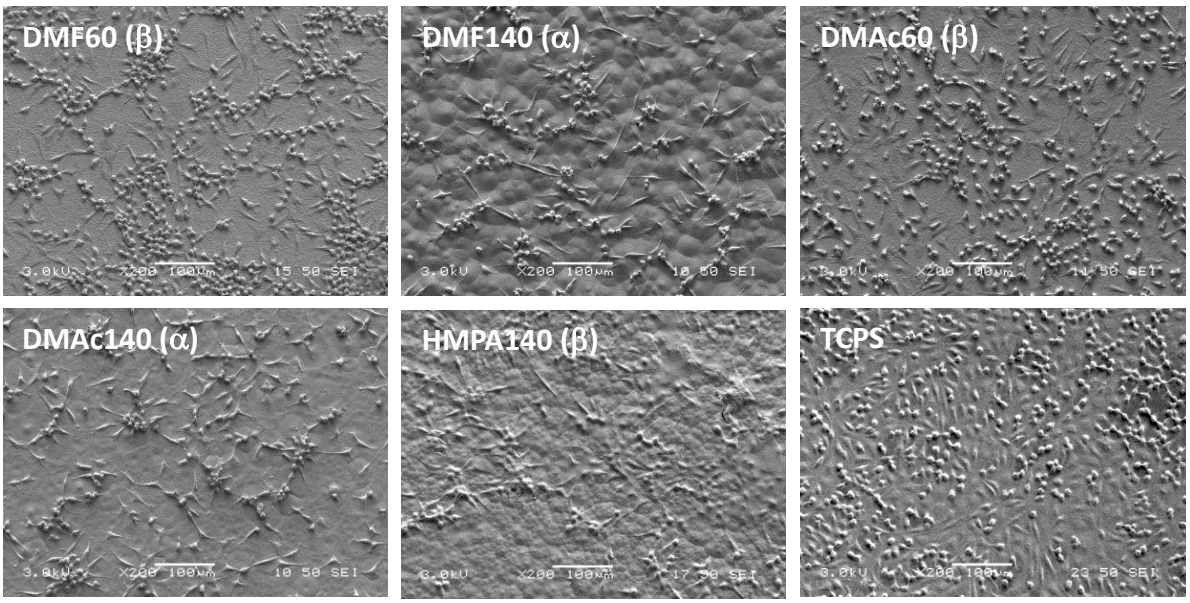
DMF60 (β)
DMF140 (α)
DMAc60 (β)
DMAc140 (α)
HMPA140 (β)
TCPS

B

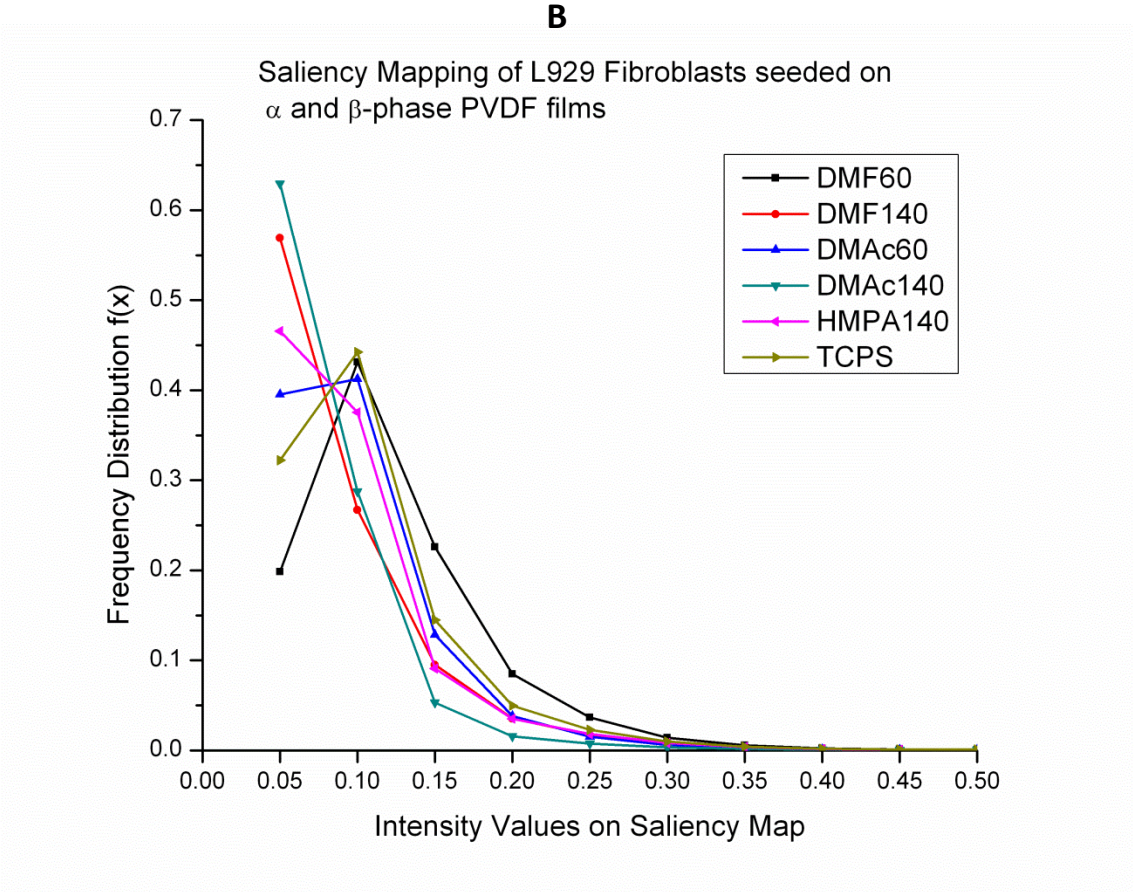
Saliency Mapping of L929 Fibroblasts seeded on
α and β-phase PVDF films
DMF60
DMF140
DMAc60
DMAc140
HMPA140
TCPS
Frequency Distribution f(x)
0.0
0.1
0.2
0.3
0.4
0.5
0.6
0.7
0.00
0.05
0.10
0.15
0.20
0.25
0.30
0.35
0.40
0.45
0.50
Intensity Values on Saliency Map

Figure 6

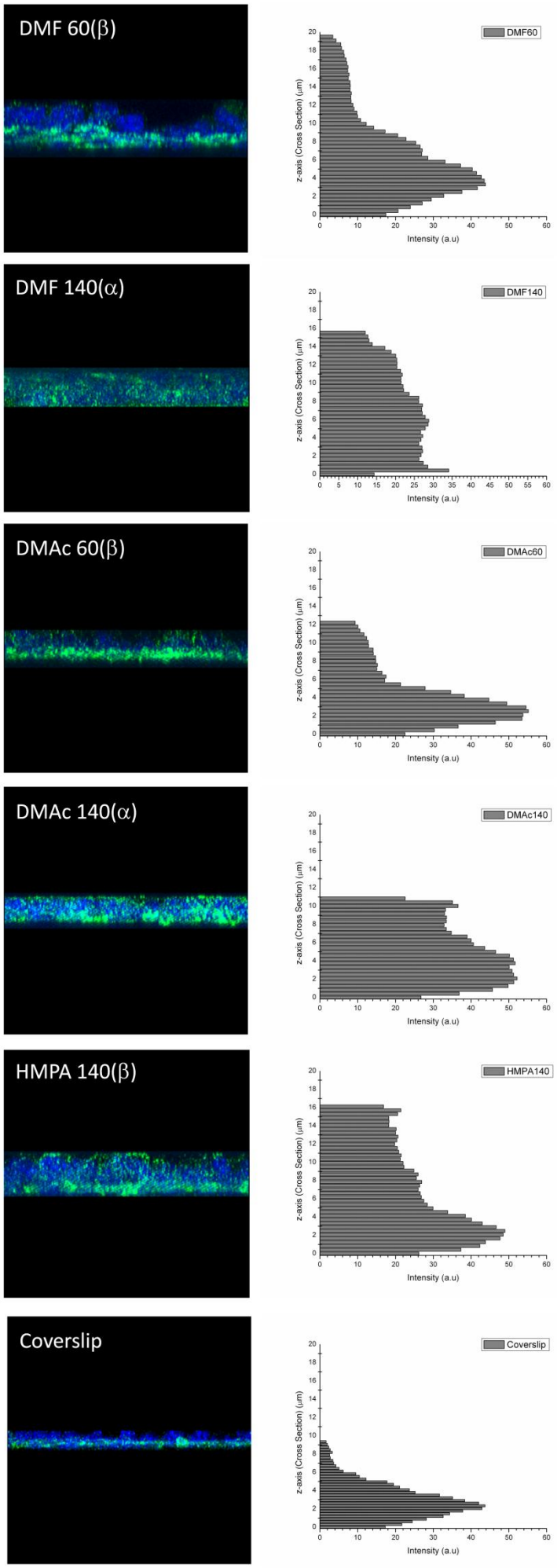
DMF 60(β)
DMF60
DMF 140(α)
DMF140
DMAc 60(β)
DMAc60
DMAc 140(α)
DMAc140
HMPA 140(β)
HMPA140
Coverslip
Coverslip
z-axis (Cross Section) (μm)
Intensity (a.u)

Authors' pictures

Vitae

Low Yuen Kei Adarina

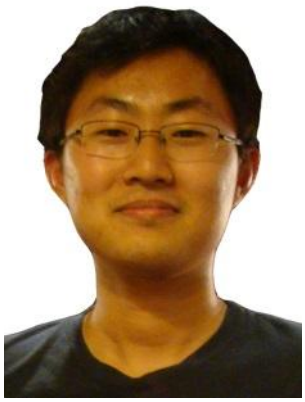

Zou Xi

Fang Yuming

Wang Junling

Lin Weisi

Freddy Boey Yin Chiang

Ng Kee Woei